

Assessment of Charge-Transfer Excitations in Organic Dyes obtained from TD-srDFT Based on Long-Range MP2 and MCSCF Wave Functions

Erik Donovan Hedegård,^{1, a)} Frank Heiden,¹ Stefan Knecht,^{1, 2} Emmanuel Fromager,³ and Hans Jørgen Aagaard Jensen^{1, b)}

¹⁾ *Department of Physics, Chemistry and Pharmacy, University of Southern Denmark, Odense, Denmark*

²⁾ *Laboratory of Physical Chemistry, ETH Zürich, Wolfgang-Pauli-Str. 10, CH-8093 Zürich, Switzerland*

³⁾ *Laboratoire de Chimie Quantique, Institut de Chimie, CNRS et Université de Strasbourg, 4 rue Blaise Pascal, 67000 Strasbourg, France*

(Dated: 23 November 2021)

Charge transfer excitations can be described within Time-Dependent Density Functional Theory (TD-DFT), not only by means of long-range corrected exchange functionals but also with a combination of wave function theory and TD-DFT based on range separation. The latter approach enables a rigorous formulation of multi-determinantal TD-DFT schemes where excitation classes, which are absent in conventional TD-DFT spectra (like for example double excitations), can be addressed. This paper investigates the combination of both the long-range *Multi-Configuration Self-Consistent Field* (MCSCF) and *Second Order Polarization Propagator Approximation* (SOPPA) *ansätze* with a short-range DFT (srDFT) description. We find that the combinations of SOPPA or MCSCF with TD-DFT yield better results than could be expected from the pure wave function schemes. For the Time-Dependent MCSCF short-range DFT *ansatz* (TD-MC-srDFT) excitation energies calculated over a larger benchmark set of molecules with predominantly single reference character yield good agreement with their reference values, and are in general comparable to the long-range corrected functional CAM-B3LYP. The SOPPA-srDFT scheme is tested for a subset of molecules used for benchmarking TD-MC-srDFT and performs slightly better against the reference data for this small subset. Beyond the proof-of-principle calculations comprising the first part of this contribution, we additionally studied the low-lying singlet excited states (S_1 and S_2) of the retinal chromophore. The chromophore displays multireference character in the ground state and both excited states exhibit considerable double excitation character, which in turn cannot be described within standard TD-DFT, due to the adiabatic approximation. However, a TD-MC-srDFT approach can account for the multireference character, and excitation energies are obtained with accuracy comparable to CASPT2, although using a much smaller active space.

PACS numbers: Valid PACS appear here

Keywords: TD-DFT, range separation, Multi-configuration methods, SOPPA-srDFT, charge transfer, peptides, retinal, TD-MC-srDFT

I. INTRODUCTION

The energy absorption in the electronic excitations wave number regime is the basis for numerous industrial applications such as dye-sensitized solar cells and artificial photo synthesis^{1,2}. In these areas, theoretical chemistry holds a great potential in the prediction and fine tuning of new molecular building blocks for novel materials. To link experiment with theory, it is of utmost importance to have methods at hand which can predict accurate electron excitation energies for several excitation classes within a given molecule.

The success of Time-Dependent Density Functional Theory (TD-DFT) in this area³⁻⁵ relies on its accuracy and computational efficiency for excitations occurring between orbitals within a functional group or between functional groups in close proximity to each other. Such ex-

citations are typically referred to as the class of *local excitations*. Other examples of excitation classes are Rydberg and Charge Transfer (CT) excitations. For these types of excitations TD-DFT is known to exhibit shortcomings: Rydberg excitations are notoriously underestimated due to the wrong asymptotic behavior of most Generalized Gradient Approximated (GGA) DFT functionals. Also CT excitations are often severely underestimated by TD-DFT⁶⁻⁹. A detailed study by Dreuw and Head-Gordon in 2004¹⁰ showed that regular exchange-correlation density-functionals display a wrong behavior of CT states with respect to the distance between the separated charges and it was argued that this feature is inherently caused by a self-interaction error arising through the electron transfer in the CT state, ultimately leading to underestimated CT excitation energies. Errors in Rydberg excitations can to some degree be remedied by asymptotically corrected functionals, and new functionals have also been proposed to meet the challenges for CT excitations. Examples include the range-separated hybrid functionals¹¹⁻¹³ such as CAM-B3LYP¹⁴

^{a)} Electronic mail: edh@sdu.dk

^{b)} Electronic mail: hjj@sdu.dk

that rely on the separation of the two-electron repulsion $1/r_{12}$ into long- and short-range parts for the calculation of the exchange energy. The above-mentioned developments have been driven by modifying exchange functionals to meet the requirements within the various excitation classes. However, TD-DFT still exhibits some fundamental flaws, which are difficult to overcome in the conventional single-configuration Kohn-Sham (KS) framework. For instance, for compounds with significant amount of multireference character and/or with excitations which have a high degree of double excitation character, TD-DFT will generally fail within the adiabatic approximation,^{15–18} which is the standard approach in most quantum chemistry codes today. Suitable methods such as the *Multi-Configuration Self-Consistent Field* (MCSCF) approach suffer on the other hand from a neglect of large parts of the local dynamical correlation which has to be recovered in a subsequent step. Popular approaches to achieve this goal are mainly based on multireference perturbation theory and we shall here mention *second-order Complete Active Space perturbation theory* (CASPT2)^{19,20} and *second-order N-electron valence state perturbation theory* (NEVPT2)²¹. Nevertheless, these methods are already computationally expensive whereas more accurate multireference Configuration Interaction (MRCI) or Coupled Cluster (MRCC) schemes are even more restricted due to their steep exponential scaling with system size.

An appealing alternative consists thus in coupling wave function theory (WFT) with DFT where the latter accounts for the major part of the dynamical correlation. There have been several suggestions for how such a scheme could be devised, e.g. the DFT/MRCI method developed by Grimme and co-workers^{22,23}. We focus in this work on the so-called long-range WFT / short-range DFT (WFT-srDFT) approach for which long-range Hartree-Fock (HF) and post-HF approximations have been developed in recent years by various research groups. Currently, the methods HF-srDFT²⁴, *Second-order Møller-Plesset* srDFT (MP2-srDFT)^{24,25}, CI-srDFT²⁶, CC-srDFT²⁷, MC-srDFT^{28,29} and NEVPT2-srDFT³⁰ have been presented. The extension to the time-dependent linear response regime has been explored initially by Pernal³¹ who described long-range correlation effects within one-electron reduced density-matrix theory. Very recently time-dependent versions of HF-srDFT^{32,33} and MC-srDFT schemes³² have been implemented. We denote these time-dependent methods TD-HF-srDFT and TD-MC-srDFT, respectively.

In this work we investigate the performance of the TD-MC-srDFT method for calculation of local and CT excitations in organic dyes. Comparison is made with standard TD-DFT results, obtained with the regular hybrid B3LYP and the long-range corrected hybrid CAM-B3LYP functionals. We further introduce the SOPPA-srDFT scheme, whose formulation is based on a long-range MP2 expansion of the TD-MC-srDFT³² linear re-

sponse equations. The SOPPA-srDFT method is tested against a subset of the molecules used to benchmark TD-MC-srDFT. As a final application, we investigate the performance of the TD-MC-srDFT method for the retinal chromophore, for which CASPT2 has been the standard method of choice for long³⁴. The theory behind the TD-MC-srDFT and SOPPA-srDFT methods are summarized in the following section (Section II), while computational details for the benchmark set of molecules and the retinal chromophore are given in Section III. All results are described in Section IV, and conclusions are given in the final section (Section V).

II. THEORY

A. Range-separated density-functional theory

The multi-determinantal extensions of TD-DFT considered in this work rely on the range separation of the regular two-electron repulsion³⁵

$$|\mathbf{r} - \mathbf{r}'|^{-1} = w_{ee}^{\text{lr},\mu}(|\mathbf{r} - \mathbf{r}'|) + w_{ee}^{\text{sr},\mu}(|\mathbf{r} - \mathbf{r}'|), \quad (1)$$

where the long-range interaction based on the error function is used,

$$w_{ee}^{\text{lr},\mu}(|\mathbf{r} - \mathbf{r}'|) = \frac{\text{erf}(\mu|\mathbf{r} - \mathbf{r}'|)}{|\mathbf{r} - \mathbf{r}'|}, \quad (2)$$

and μ is the parameter that controls the range separation. The exact ground-state energy of an electronic system can then in principle be obtained variationally as follows

$$E = \min_{\Psi} \left\{ \langle \Psi | \hat{T} + \hat{W}_{ee}^{\text{lr},\mu} | \Psi \rangle + E_{\text{Hxc}}^{\text{sr},\mu}[\rho_{\Psi}] + \int d\mathbf{r} v_{\text{ne}}(\mathbf{r})\rho_{\Psi}(\mathbf{r}) \right\}, \quad (3)$$

where \hat{T} and $\hat{W}_{ee}^{\text{lr},\mu}$ are the kinetic energy and long-range two-electron interaction operators, respectively, while $v_{\text{ne}}(\mathbf{r})$ denotes the local nuclear potential. The μ -dependent complementary density-functional $E_{\text{Hxc}}^{\text{sr},\mu}[\rho]$ can be split into short-range Hartree, exchange and correlation (srHxc) contributions

$$E_{\text{Hxc}}^{\text{sr},\mu}[\rho] = E_{\text{H}}^{\text{sr},\mu}[\rho] + E_{\text{x}}^{\text{sr},\mu}[\rho] + E_{\text{c}}^{\text{sr},\mu}[\rho], \quad (4)$$

where $E_{\text{H}}^{\text{sr},\mu}[\rho] = \frac{1}{2} \int \int d\mathbf{r} d\mathbf{r}' \rho(\mathbf{r})\rho(\mathbf{r}')w_{ee}^{\text{sr},\mu}(|\mathbf{r} - \mathbf{r}'|)$. The usual expression for the exact short-range exchange energy $E_{\text{x}}^{\text{sr},\mu}[\rho] = \langle \Phi^{\text{KS}}[\rho] | \hat{W}_{ee}^{\text{sr},\mu} | \Phi^{\text{KS}}[\rho] \rangle$ is, as in standard DFT, based on the KS determinant. This definition has been used by Savin and co-workers³⁶ for constructing approximate short-range exchange and correlation density-functionals. The exact minimizing wave function Ψ^{μ} in Eq. (3) is the ground state of the long-range interacting system whose density $\rho^{\mu}(\mathbf{r}) = \langle \Psi^{\mu} | \hat{\rho}(\mathbf{r}) | \Psi^{\mu} \rangle$ equals the density of the physical fully-interacting system. It fulfills

the self-consistent equation

$$\hat{H}^\mu[\rho^\mu]|\Psi^\mu\rangle = \mathcal{E}^\mu|\Psi^\mu\rangle, \quad (5)$$

where the density-dependent long-range Hamiltonian equals

$$\begin{aligned} \hat{H}^\mu[\rho] &= \hat{T} + \hat{W}_{\text{ee}}^{\text{lr},\mu} + \hat{V}_{\text{ne}} + \hat{V}_{\text{Hxc}}^{\text{sr},\mu}[\rho], \\ \hat{V}_{\text{Hxc}}^{\text{sr},\mu}[\rho] &= \int d\mathbf{r} \frac{\delta E_{\text{Hxc}}^{\text{sr},\mu}}{\delta \rho(\mathbf{r})}[\rho] \hat{\rho}(\mathbf{r}), \end{aligned} \quad (6)$$

and $\hat{V}_{\text{ne}} = \int d\mathbf{r} v_{\text{ne}}(\mathbf{r}) \hat{\rho}(\mathbf{r})$. Since the long-range interaction is treated explicitly, in contrast to KS-DFT, the exact solution is multi-determinantal. The approximate range-separated DFT models considered in this work describe the long-range interaction at the HF, MP2 and MCSCF levels. These schemes will be referred to as HF-srDFT, MP2-srDFT and MC-srDFT, respectively. Their extensions to the time-dependent linear response regime is presented in the following.

B. Extension to the time-dependent regime

As discussed in details in Ref. 32, excited-state properties can be described when extending Eqs. (3) and (5) to the time-dependent regime. Within the short-range adiabatic approximation³², the time evolution of the auxiliary long-range interacting system is obtained as follows

$$\begin{aligned} \left(\hat{T} + \hat{W}_{\text{ee}}^{\text{lr},\mu} + \hat{V}(t) + \hat{V}_{\text{Hxc}}^{\text{sr},\mu}[\tilde{\rho}^\mu(\mathbf{r}, t)] - i \frac{\partial}{\partial t} \right) |\tilde{\Psi}^\mu(t)\rangle \\ = Q^\mu(t) |\tilde{\Psi}^\mu(t)\rangle, \end{aligned} \quad (7)$$

where $\tilde{\rho}^\mu(\mathbf{r}, t) = \langle \tilde{\Psi}^\mu(t) | \hat{\rho}(\mathbf{r}) | \tilde{\Psi}^\mu(t) \rangle$ is an approximation to the exact time-dependent density of the physical fully-interacting system and $\hat{V}(t) = \int d\mathbf{r} v(\mathbf{r}, t) \hat{\rho}(\mathbf{r})$ is a local time-dependent potential operator. If the latter is periodic of period T , Eq. (7) is equivalent to the variational principle

$$\delta Q^\mu[\tilde{\Psi}^\mu] = 0, \quad (8)$$

which is formulated in terms of the range-separated wave function-dependent action integral

$$\begin{aligned} Q^\mu[\Psi] &= \int_0^T dt \frac{\langle \Psi(t) | \hat{T} + \hat{W}_{\text{ee}}^{\text{lr},\mu} + \hat{V}(t) - i \frac{\partial}{\partial t} | \Psi(t) \rangle}{\langle \Psi(t) | \Psi(t) \rangle} \\ &+ \int_0^T dt E_{\text{Hxc}}^{\text{sr},\mu}[\rho_{\Psi(t)}]. \end{aligned} \quad (9)$$

The linear response TD-MC-srDFT model discussed in the following is based on the variational formulation in Eq. (8).

C. TD-MC-srDFT model

We work in this section in the framework of Floquet theory³⁷ where the time-dependent periodic perturbation is decomposed as follows

$$\begin{aligned} \hat{V}(t) &= \hat{V}_{\text{ne}} + \sum_x \sum_{k=-N}^N e^{-i\omega_k t} \varepsilon_x(\omega_k) \hat{V}_x, \\ \omega_k &= \frac{2\pi k}{T}, \end{aligned} \quad (10)$$

$$\hat{V}_x = \int d\mathbf{r} v_x(\mathbf{r}) \hat{\rho}(\mathbf{r}).$$

We use a MCSCF parametrization of the time-dependent wave function $\tilde{\Psi}^\mu(t) \rightarrow |\tilde{0}^\mu(t)\rangle$ in Eq. (8) consisting of exponential unitary transformations³⁸

$$|\tilde{0}^\mu(t)\rangle = e^{i\hat{\kappa}(t)} e^{i\hat{S}(t)} |0^\mu\rangle, \quad (11)$$

which are applied to the unperturbed MC-srDFT wave function $|0^\mu\rangle$ with

$$\begin{aligned} \hat{\kappa}(t) &= \sum_{l,i} e^{-i\omega_l t} \kappa_i(\omega_l) \hat{q}_i^\dagger + e^{-i\omega_l t} \kappa_i^*(-\omega_l) \hat{q}_i, \\ \hat{S}(t) &= \sum_{l,i} e^{-i\omega_l t} S_i(\omega_l) \hat{R}_i^\dagger + e^{-i\omega_l t} S_i^*(-\omega_l) \hat{R}_i. \end{aligned} \quad (12)$$

The singlet excitation and state-transfer operators are defined as follows

$$\begin{aligned} \hat{q}_i^\dagger &= \hat{E}_{pq} = \hat{a}_{p\alpha}^\dagger \hat{a}_{q\alpha} + \hat{a}_{p\beta}^\dagger \hat{a}_{q\beta}; \quad p > q, \\ \hat{R}_i^\dagger &= |i\rangle \langle 0^\mu|. \end{aligned} \quad (13)$$

Note that the TD-HF-srDFT scheme is a particular case of Eq. (11), where the unperturbed MC-srDFT wave function would be replaced by the HF-srDFT determinant, and only orbital rotations would be considered. Returning to the multi-configuration case, the TD-MC-srDFT wave function in Eq. (11) is fully determined by the Fourier component vectors

$$\Lambda(\omega_l) = \begin{bmatrix} \kappa_i(\omega_l) \\ S_i(\omega_l) \\ \kappa_i^*(-\omega_l) \\ S_i^*(-\omega_l) \end{bmatrix}, \quad (14)$$

for which we consider in the following the Taylor expansion through first order:

$$\Lambda(\omega_l) = \sum_{k=-N,x}^N \varepsilon_x(\omega_k) \left. \frac{\partial \Lambda(\omega_l)}{\partial \varepsilon_x(\omega_k)} \right|_{\varepsilon=0} + \dots \quad (15)$$

Rewriting the variational condition in Eq. (8) as follows

$$\forall \varepsilon_x(\omega_k) \quad \frac{\partial Q^\mu}{\partial \Lambda^\dagger(-\omega_l)} = 0, \quad (16)$$

the linear response equations are simply obtained by differentiation with respect to the perturbation strength $\varepsilon_x(\omega_k)$ ³²:

$$\left(\frac{d}{d\varepsilon_x(\omega_k)} \frac{\partial \mathcal{Q}^\mu}{\partial \Lambda^\dagger(-\omega_l)} \right) \Big|_{\varepsilon=0} = 0, \quad (17)$$

which leads, according to Eq. (9) and Refs. 32 and 39, to

$$\begin{aligned} \left(\frac{d}{d\varepsilon_x(\omega_k)} \frac{\partial \mathcal{Q}^\mu}{\partial \Lambda^\dagger(-\omega_l)} \right) \Big|_{\varepsilon=0} &= \frac{d}{d\varepsilon_x(\omega_k)} \frac{\partial}{\partial \Lambda^\dagger(-\omega_l)} \\ &\left(\frac{T}{2} \sum_{m,n} \delta(\omega_m + \omega_n) \right. \\ &\quad \times \Lambda^\dagger(-\omega_m) \left[E_0^{[2]\mu} + K_{\text{Hxc}}^{\text{sr},\mu} + \omega_m S^{[2]\mu} \right] \Lambda(\omega_n) \quad (18) \\ &\quad \left. + \frac{T}{2} \sum_m \sum_y \sum_{p=-N}^N \delta(\omega_m + \omega_p) \varepsilon_y(\omega_p) \right. \\ &\quad \left. \times \left[iV_y^{[1]\mu\dagger} \Lambda(\omega_m) - i\Lambda^\dagger(-\omega_m) V_y^{[1]\mu} \right] \right) \Big|_{\varepsilon=0} = 0. \end{aligned}$$

Several matrices and vectors have been introduced in Eq. (18). First are the long-range Hessian, $E_0^{[2]\mu}$, the srHxc kernel, $K_{\text{Hxc}}^{\text{sr},\mu}$, and μ -dependent metric $S^{[2]\mu}$. These matrices will along with the property gradient vector, $V_y^{[1]\mu}$ be described in more detail below: The long-range Hessian ($E_0^{[2]\mu}$) is obtained from the auxiliary Hamiltonian $\hat{H}_0^\mu = \hat{H}^\mu[\rho_0^\mu]$, that is calculated for the unperturbed MC-srDFT density $\rho_0^\mu(\mathbf{r}) = \langle 0^\mu | \hat{\rho}(\mathbf{r}) | 0^\mu \rangle$, as follows

$$E_0^{[2]\mu} = \begin{bmatrix} A^\mu & B^\mu \\ B^{\mu*} & A^{\mu*} \end{bmatrix}, \quad (19)$$

$$A^\mu = \begin{bmatrix} \langle 0^\mu | [\hat{q}_i, [\hat{H}_0^\mu, \hat{q}_j^\dagger]] | 0^\mu \rangle & \langle 0^\mu | [[\hat{q}_i, \hat{H}_0^\mu], \hat{R}_j^\dagger] | 0^\mu \rangle \\ \langle 0^\mu | [\hat{R}_i, [\hat{H}_0^\mu, \hat{q}_j^\dagger]] | 0^\mu \rangle & \langle 0^\mu | [\hat{R}_i, [\hat{H}_0^\mu, \hat{R}_j^\dagger]] | 0^\mu \rangle \end{bmatrix}, \quad (20)$$

$$B^\mu = \begin{bmatrix} \langle 0^\mu | [\hat{q}_i, [\hat{H}_0^\mu, \hat{q}_j]] | 0^\mu \rangle & \langle 0^\mu | [[\hat{q}_i, \hat{H}_0^\mu], \hat{R}_j] | 0^\mu \rangle \\ \langle 0^\mu | [\hat{R}_i, [\hat{H}_0^\mu, \hat{q}_j]] | 0^\mu \rangle & \langle 0^\mu | [\hat{R}_i, [\hat{H}_0^\mu, \hat{R}_j]] | 0^\mu \rangle \end{bmatrix},$$

and the μ -dependent metric equals

$$S^{[2]\mu} = \begin{bmatrix} \Sigma^\mu & \Delta^\mu \\ -\Delta^{\mu*} & -\Sigma^{\mu*} \end{bmatrix}, \quad (21)$$

$$\Sigma^\mu = \begin{bmatrix} \langle 0^\mu | [\hat{q}_i, \hat{q}_j^\dagger] | 0^\mu \rangle & \langle 0^\mu | [\hat{q}_i, \hat{R}_j^\dagger] | 0^\mu \rangle \\ \langle 0^\mu | [\hat{R}_i, \hat{q}_j^\dagger] | 0^\mu \rangle & \langle 0^\mu | [\hat{R}_i, \hat{R}_j^\dagger] | 0^\mu \rangle \end{bmatrix}, \quad (22)$$

$$\Delta^\mu = \begin{bmatrix} \langle 0^\mu | [\hat{q}_i, \hat{q}_j] | 0^\mu \rangle & \langle 0^\mu | [\hat{q}_i, \hat{R}_j] | 0^\mu \rangle \\ \langle 0^\mu | [\hat{R}_i, \hat{q}_j] | 0^\mu \rangle & \langle 0^\mu | [\hat{R}_i, \hat{R}_j] | 0^\mu \rangle \end{bmatrix}.$$

The srHxc kernel contribution in Eq. (18) is calculated for the unperturbed MC-srDFT density,

$$K_{\text{Hxc}}^{\text{sr},\mu} = \int \int d\mathbf{r} d\mathbf{r}' K_{\text{Hxc}}^{\text{sr},\mu}[\rho_0^\mu](\mathbf{r}, \mathbf{r}') \rho^{[1]\mu}(\mathbf{r}) \rho^{[1]\mu\dagger}(\mathbf{r}'), \quad (23)$$

$$K_{\text{Hxc}}^{\text{sr},\mu}[\rho](\mathbf{r}, \mathbf{r}') = \frac{\delta^2 E_{\text{Hxc}}^{\text{sr},\mu}}{\delta \rho(\mathbf{r}) \delta \rho(\mathbf{r}')},$$

and (as seen in Eq. 23 above), expressed in terms of the gradient density vector

$$\rho^{[1]\mu}(\mathbf{r}) = \begin{bmatrix} \langle 0^\mu | [\hat{q}_i, \hat{\rho}(\mathbf{r})] | 0^\mu \rangle \\ \langle 0^\mu | [\hat{R}_i, \hat{\rho}(\mathbf{r})] | 0^\mu \rangle \\ \langle 0^\mu | [\hat{q}_j^\dagger, \hat{\rho}(\mathbf{r})] | 0^\mu \rangle \\ \langle 0^\mu | [\hat{R}_j^\dagger, \hat{\rho}(\mathbf{r})] | 0^\mu \rangle \end{bmatrix}. \quad (24)$$

Finally, the gradient property vector equals

$$V_y^{[1]\mu} = \int d\mathbf{r} v_y(\mathbf{r}) \rho^{[1]\mu}(\mathbf{r}). \quad (25)$$

The linear response equations (Eq. 18) can now be rewritten in a compact form as follows

$$\left(E^{[2]\mu} + \omega_l S^{[2]\mu} \right) \frac{\partial \Lambda(-\omega_l)}{\partial \varepsilon_x(\omega_k)} \Big|_{\varepsilon=0} = iV_x^{[1]\mu} \delta(\omega_k + \omega_l), \quad (26)$$

or, equivalently,

$$\left(E^{[2]\mu} - \omega_l S^{[2]\mu} \right) \frac{\partial \Lambda(\omega_l)}{\partial \varepsilon_x(\omega_k)} \Big|_{\varepsilon=0} = iV_x^{[1]\mu} \delta(\omega_k - \omega_l), \quad (27)$$

where the MC-srDFT Hessian is comprised of the long-range Hessian and the Hxc kernel from Eqs. (19) and (23)

$$E^{[2]\mu} = E_0^{[2]\mu} + K_{\text{Hxc}}^{\text{sr},\mu}. \quad (28)$$

Note that in Eq. (38) of Ref. 32 the metric that was used is the one in Eq. (21) multiplied by -1, as in Ref. 39. This is why the metric is multiplied by $+\omega_l$ in Eq. (26) instead of $-\omega_l$ as done in Ref. 32.

The time-dependent expectation value of the perturbation can thus be expanded through first order

$$\begin{aligned} \langle \tilde{0}^\mu(t) | \hat{V}_y | \tilde{0}^\mu(t) \rangle &= \langle 0^\mu | \hat{V}_y | 0^\mu \rangle \\ &+ i \sum_l e^{-i\omega_l t} V_y^{[1]\mu\dagger} \sum_x \sum_{k=-N}^N \varepsilon_x(\omega_k) \frac{\partial \Lambda(\omega_l)}{\partial \varepsilon_x(\omega_k)} \Big|_{\varepsilon=0} \\ &+ \dots \quad (29) \end{aligned}$$

$$\begin{aligned} &= \langle 0^\mu | \hat{V}_y | 0^\mu \rangle + \sum_x \sum_{k=-N}^N e^{-i\omega_k t} \varepsilon_x(\omega_k) \langle \langle \hat{V}_y, \hat{V}_x \rangle \rangle_{\omega_k} \\ &+ \dots, \end{aligned}$$

where, according to Eq. (27), the linear response function

equals

$$\langle\langle \hat{V}_y, \hat{V}_x \rangle\rangle_{\omega_k} = -V_y^{[1]\mu\dagger} \left[E^{[2]\mu} - \omega_k S^{[2]\mu} \right]^{-1} V_x^{[1]\mu}. \quad (30)$$

Excitation energies ω_I can then be calculated at the TD-MC-srDFT level when solving iteratively

$$\left(E^{[2]\mu} - \omega_I S^{[2]\mu} \right) X(\omega_I) = 0. \quad (31)$$

The linear response function in Eq. (30) can *formally* be re-expressed in the basis of the converged solutions $X(\omega_I)$ which leads to³⁸

$$\langle\langle \hat{V}_y, \hat{V}_x \rangle\rangle_{\omega_k} = - \sum_I \frac{f_I^{yx}}{\omega_I^2 - \omega_k^2}, \quad (32)$$

where the oscillator strengths are determined as follows

$$f_I^{yx} = 2\omega_I (X^\dagger(\omega_I) V_y^{[1]\mu})^\dagger X^\dagger(\omega_I) V_x^{[1]\mu}. \quad (33)$$

The last three equations (Eqs. 30–33) comprise the ingredients for calculation of excitation energies and intensities within the TD-MC-srDFT scheme.

D. SOPPA-srDFT model

As an alternative to TD-MC-srDFT for systems which are not strongly multi-configurational, the SOPPA-srDFT scheme will now be introduced. It consists of an application of the SOPPA approach^{40,41} to the auxiliary long-range interacting system. For that purpose we will replace in the TD-MC-srDFT linear response Eq. (27) the unperturbed MC-srDFT wave function $|0^\mu\rangle$ by a Møller-Plesset (MP) perturbation expansion through second order in the long-range fluctuation potential^{25,42}

$$|0^\mu\rangle \rightarrow |\text{HF}^\mu\rangle + |0^{(1)\text{lr},\mu}\rangle + |0^{(2)\mu}\rangle + \dots, \quad (34)$$

where $|\text{HF}^\mu\rangle$ denotes the HF-srDFT determinant. The first-order contribution is the analog of the standard MP1 wave function correction based on the long-range Hamiltonian $\hat{H}^\mu[\rho_{\text{HF}}^\mu]$ that is calculated for the HF-srDFT density ρ_{HF}^μ , while the second-order term includes self-consistency effects²⁵. Based on the analysis and numerical results of Fromager and Jensen⁴², where it was shown that these effects can be safely neglected through second order, self-consistency will be not be included in the presented SOPPA-srDFT results. According to the Brillouin theorem the density remains unchanged through first order which explains why self-consistency only appears through second order in the wave function. The density can therefore be expanded as

$$\rho_0^\mu(\mathbf{r}) \rightarrow \rho_{\text{HF}}^\mu(\mathbf{r}) + \delta\rho^{(2)\mu}(\mathbf{r}) + \dots \quad (35)$$

The SOPPA-srDFT equations are then obtained when expanding the linear response Eq. (27) through second order in the long-range fluctuation potential. The $|D_i\rangle\langle\text{HF}^\mu|$ operator corresponds to what in the original

SOPPA literature is denoted the two-particle-two-hole operator. Since one and two particle-hole manifolds are sufficient to define the SOPPA response⁴¹, the orbital and configuration rotation operators can be written as

$$\begin{aligned} \hat{q}_i^\dagger &\rightarrow \hat{E}_{ai} \\ \hat{R}_i^\dagger &\rightarrow |D_i\rangle\langle\text{HF}^\mu|, \end{aligned} \quad (36)$$

where i and a are occupied and unoccupied HF-srDFT orbitals, respectively, while $|D_i\rangle$ denote singlet and triplet doubly-excited states. Since the metric and the gradient property vector in Eq. (27) depend on the wave function through expectation values only (see Eqs. (21), (22) and (24)), their expressions in SOPPA-srDFT are obtained from standard SOPPA when replacing the regular Hamiltonian by $\hat{H}^\mu[\rho_{\text{HF}}^\mu]$, as self-consistency effects on the wave function are neglected through second order.

The derivation of the Hessian requires more discussion as it also depends on the density through the srHxc potential and kernel. Note that, in order to obtain the correct linear response function through second order, the Hessian matrix elements should be computed through second order in the orbital-orbital blocks, first order in the orbital-configuration blocks and zeroth order in the configuration-configuration blocks⁴¹. According to Eq. (35), the long-range interacting Hamiltonian in Eq. (20) is expanded through second order as follows

$$\begin{aligned} \hat{H}_0^\mu &\rightarrow \hat{H}^\mu[\rho_{\text{HF}}^\mu] \\ &+ \int \int d\mathbf{r}d\mathbf{r}' K_{\text{Hxc}}^{\text{sr},\mu}[\rho_{\text{HF}}^\mu](\mathbf{r}, \mathbf{r}') \delta\rho^{(2)\mu}(\mathbf{r}) \hat{\rho}(\mathbf{r}') \\ &+ \dots \end{aligned} \quad (37)$$

The second-order correction in Eq. (37) needs to be considered in the orbital-orbital blocks of the Hessian only, leading to the following contribution for the upper left block

$$\begin{aligned} &\int \int d\mathbf{r}d\mathbf{r}' K_{\text{Hxc}}^{\text{sr},\mu}[\rho_{\text{HF}}^\mu](\mathbf{r}, \mathbf{r}') \delta\rho^{(2)\mu}(\mathbf{r}) \\ &\times \langle\text{HF}^\mu| [\hat{E}_{ia}, [\hat{\rho}(\mathbf{r}'), \hat{E}_{bj}]] |\text{HF}^\mu\rangle \\ &= 2 \int \int d\mathbf{r}d\mathbf{r}' K_{\text{Hxc}}^{\text{sr},\mu}[\rho_{\text{HF}}^\mu](\mathbf{r}, \mathbf{r}') \delta\rho^{(2)\mu}(\mathbf{r}) \\ &\times \left(\delta_{ij} \Omega_{ab}(\mathbf{r}') - \delta_{ab} \Omega_{ij}(\mathbf{r}') \right), \end{aligned} \quad (38)$$

where $\Omega_{pq}(\mathbf{r}) = \phi_p(\mathbf{r})\phi_q(\mathbf{r})$ denotes the product of HF-srDFT orbitals. Let us now consider the srHxc kernel contribution to the Hessian in Eq. (23) that is determined from the following perturbation expansion through second order

$$\begin{aligned} K_{\text{Hxc}}^{\text{sr},\mu}[\rho_0^\mu](\mathbf{r}, \mathbf{r}') &\rightarrow K_{\text{Hxc}}^{\text{sr},\mu}[\rho_{\text{HF}}^\mu](\mathbf{r}, \mathbf{r}') \\ &+ \int d\mathbf{r}'' \frac{\delta K_{\text{Hxc}}^{\text{sr},\mu}}{\delta\rho(\mathbf{r}'')}[\rho_{\text{HF}}^\mu](\mathbf{r}, \mathbf{r}') \delta\rho^{(2)\mu}(\mathbf{r}'') \\ &+ \dots \end{aligned} \quad (39)$$

The second-order term in Eq. (39) should be considered

in the orbital-orbital blocks only, leading to the following contribution in the upper left block

$$\begin{aligned} & \int \int \int \mathrm{d}\mathbf{r}\mathrm{d}\mathbf{r}'\mathrm{d}\mathbf{r}'' \frac{\delta K_{\mathrm{Hxc}}^{\mathrm{sr},\mu}}{\delta \rho(\mathbf{r}'')} [\rho_{\mathrm{HF}}^\mu](\mathbf{r}, \mathbf{r}') \delta \rho^{(2)\mu}(\mathbf{r}'') \\ & \times \langle \mathrm{HF}^\mu | [\hat{E}_{ia}, \hat{\rho}(\mathbf{r})] | \mathrm{HF}^\mu \rangle \langle \mathrm{HF}^\mu | [\hat{\rho}(\mathbf{r}'), \hat{E}_{bj}] | \mathrm{HF}^\mu \rangle \\ & = 4 \int \int \int \mathrm{d}\mathbf{r}\mathrm{d}\mathbf{r}'\mathrm{d}\mathbf{r}'' \frac{\delta K_{\mathrm{Hxc}}^{\mathrm{sr},\mu}}{\delta \rho(\mathbf{r}'')} [\rho_{\mathrm{HF}}^\mu](\mathbf{r}, \mathbf{r}') \delta \rho^{(2)\mu}(\mathbf{r}'') \\ & \quad \times \Omega_{ai}(\mathbf{r}) \Omega_{bj}(\mathbf{r}'). \end{aligned} \quad (40)$$

The remaining contributions to the Hessian that have to be considered arise from the srHxc kernel calculated with the HF-srDFT density

$$\int \int \mathrm{d}\mathbf{r}\mathrm{d}\mathbf{r}' K_{\mathrm{Hxc}}^{\mathrm{sr},\mu} [\rho_{\mathrm{HF}}^\mu](\mathbf{r}, \mathbf{r}') \rho^{[1]\mu}(\mathbf{r}) \rho^{[1]\mu\dagger}(\mathbf{r}'), \quad (41)$$

where the perturbation expansion of the orbital components in the gradient density vector

$$\begin{aligned} \langle 0^\mu | [\hat{E}_{ia}, \hat{\rho}(\mathbf{r})] | 0^\mu \rangle &= \sum_{p,q} \Omega_{pq}(\mathbf{r}) \langle 0^\mu | [\hat{E}_{ia}, \hat{E}_{pq}] | 0^\mu \rangle \\ &= \sum_{p,q} \Omega_{pq}(\mathbf{r}) \\ & \quad \times (\delta_{ap} D_{iq}^\mu - \delta_{iq} D_{pa}^\mu), \end{aligned} \quad (42)$$

is deduced from the one-electron reduced density matrix (1RDM) expansion

$$\begin{aligned} D_{pq}^\mu &= \langle 0^\mu | \hat{E}_{pq} | 0^\mu \rangle \\ &\rightarrow \sum_i 2\delta_{ip} \delta_{iq} + D_{pq}^{(2)\mu} + \dots \end{aligned} \quad (43)$$

Note that the first-order contribution to the 1RDM is zero because of the Brillouin theorem²⁵. We thus obtain through second order

$$\begin{aligned} \langle 0^\mu | [\hat{E}_{ia}, \hat{\rho}(\mathbf{r})] | 0^\mu \rangle &\rightarrow 2\Omega_{ai}(\mathbf{r}) \\ &+ \sum_p (\Omega_{pa}(\mathbf{r}) D_{ip}^{(2)\mu} - \Omega_{pi}(\mathbf{r}) D_{pa}^{(2)\mu}) + \dots \end{aligned} \quad (44)$$

It was shown numerically by Fromager and Jensen⁴² that, for the usual $\mu = 0.4$ value, the long-range MP2 contribution to the 1RDM is relatively small as long as it is computed for systems that are not strongly multi-configurational. As a result, the second-order contributions in Eqs. (38), (40) and (44) have been neglected in our implementation. Let us finally focus on the configuration part of the gradient density vector that must be expanded through first order in order to compute the srHxc kernel orbital-configuration blocks:

$$\begin{aligned} \langle 0^\mu | [\hat{R}_i, \hat{\rho}(\mathbf{r})] | 0^\mu \rangle &\rightarrow \langle \mathrm{HF}^\mu | [\hat{R}_i, \hat{\rho}(\mathbf{r})] | 0^{(1)\mathrm{lr},\mu} \rangle + \dots \\ &= \langle D_i | \hat{\rho}(\mathbf{r}) | 0^{(1)\mathrm{lr},\mu} \rangle \\ & \quad - \rho_{\mathrm{HF}}^\mu(\mathbf{r}) \langle D_i | 0^{(1)\mathrm{lr},\mu} \rangle + \dots \end{aligned} \quad (45)$$

Rewriting the long-range MP1 wave function in the basis of the doubly-excited configurations

$$|0^{(1)\mathrm{lr},\mu}\rangle = \sum_j C_j^{(1)\mathrm{lr},\mu} |D_j\rangle, \quad (46)$$

we obtain

$$\begin{aligned} \langle 0^\mu | [\hat{R}_i, \hat{\rho}(\mathbf{r})] | 0^\mu \rangle &\rightarrow C_i^{(1)\mathrm{lr},\mu} \left(\langle D_i | \hat{\rho}(\mathbf{r}) | D_i \rangle - \rho_{\mathrm{HF}}^\mu(\mathbf{r}) \right) \\ & \quad + \sum_{j \neq i} C_j^{(1)\mathrm{lr},\mu} \langle D_i | \hat{\rho}(\mathbf{r}) | D_j \rangle. \end{aligned} \quad (47)$$

This term may contribute significantly to the Hessian when considering double excitations with an important modification of the density. For simplicity it has been neglected in this work. In summary, the SOPPA-srDFT equation that has been implemented has the same structure as the linear response TD-MC-srDFT equation. The long-range interacting Hessian $E_0^{[2]\mu}$ has been replaced by the SOPPA analog based on $\hat{H}^\mu[\rho_{\mathrm{HF}}^\mu]$ while the srHxc kernel contribution has been calculated for the HF-srDFT density with the gradient density vector simplified as follows, according to Eq. (44),

$$\rho^{[1]\mu}(\mathbf{r}) \rightarrow \begin{bmatrix} 2\Omega_{ai}(\mathbf{r}) \\ 0 \\ -2\Omega_{ai}(\mathbf{r}) \\ 0 \end{bmatrix}. \quad (48)$$

III. COMPUTATIONAL DETAILS

The set of molecules used to benchmark the TD-MC-srDFT method is shown in Figure 1. It comprises hydrogen chloride, three model peptides (a simple dipeptide, a β -dipeptide and a tripeptide) and two aromatic systems, *N*-phenyl pyrrole (PP) and 4-(*N*,*N*-dimethylamino) benzonitrile (DMABN). Excitations of local and charge transfer character for these systems have previously been investigated, as part of a larger test set introduced by Peach *et al.*⁴³ for benchmarking the three-parameter Becke-Lee-Yang-Parr functional (B3LYP) and its long-range corrected version. The long-range correction has the form of the Coulomb-attenuated method and is hence denoted CAM-B3LYP¹⁴. Many of the CT excitations in the chosen systems have been problematic for TD-DFT^{6,44,45}, but can be improved with long-range corrected functionals. In order to assure a fair comparison of our data with the values used to benchmark CAM-B3LYP, we took the geometries from the study by Peach *et al.*⁴³ As reference for the calculated excitation energies, we use for the dipeptide, β -dipeptide and tripeptide, the CASPT2 values from Serrano-André and Fülischer⁴⁶. Excitation energies for *N*-phenyl pyrrole (PP) and HCl were obtained at the linear response CC level by Peach *et al.*⁴³ Finally, reference excitation data for DMABN were taken from accurate gas phase measurements⁴⁷, thus obtaining a one-to-one correspondence between the reference values

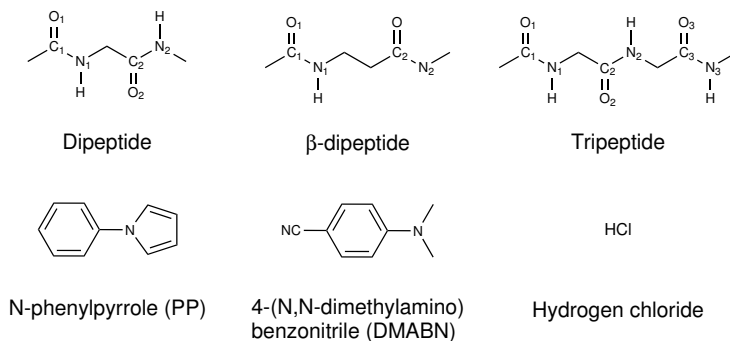


FIG. 1. Molecules used for statistical analysis.

used by Peach *et al.* and the ones adopted here. DMABN has been subject to several theoretical studies^{48,49} and CASPT2(12,12) reference values could alternatively have been used. In our calculations we use CAS(4,4) spaces for the dipeptide and β -dipeptide, while for the tripeptide, a slightly larger CAS(6,6) active space was applied. The two organic molecules (PP and DMABN) are both assigned CAS(8,8) active spaces. All calculations for the molecules in Figure 1 are carried out with a Dunning cc-pVTZ basis set⁵⁰. The srDFT calculations were performed with the spin-independent short-range exchange-correlation functional of Goll *et al.*²⁷ which is based on the Perdew-Burke-Ernzerhof (PBE) functional. It will therefore be referred to as srPBE. The μ parameter was set to $\mu = 0.4$. This value relates to a prescription given in Refs.^{28,29} where $\mu = 0.4$ was found optimal, based on an analysis of correlation effects in the MC-srPBE ground state.

The SOPPA and SOPPA-srDFT calculations were not done for the full set, but only for the smallest model peptide (dipeptide), PP and DMABN molecules. The retinal chromophore is in the all-*trans* Schiff-base form (see Figure 2). We used a structure from a very recent study⁵¹, optimized within the protein environment (using B3LYP/6-31+G*). For this system a CAS(6,6) space was

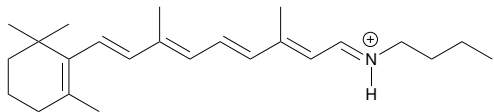


FIG. 2. Retinal chromophore (including a small part of the lysine residue which attach retinal to the channel-rhodopsin protein).

chosen based on MP2-srPBE natural orbital occupation numbers⁴². TD-srPBE calculations on retinal were performed with a 6-31G* basis set, and we have accordingly not included the results from the retinal calculations in any of the statistical analysis presented in Section IV.

All calculations were carried out using a development version of the DALTON program⁵².

IV. RESULTS AND DISCUSSION

A. Classification of Excitations

To identify whether a given excitation is of local (“L”) or of charge transfer (“CT”) character, response vectors from the calculation of excitation energies for each of the molecular systems in Figure 1 have been through a careful analysis. This includes analysis of both transitions between orbitals and configurations along with visual inspection of the orbitals involved. Results are given in Table I for the dipeptide, PP and DMABN molecules. Table II shows TD-MC-srPBE results for the remaining molecules (β -dipeptide, tripeptide and HCl). We here mainly discuss the excitations which are qualitatively different from previous benchmark results and accordingly the dipeptide, DMABN, HCl and PP molecules (which all give the same qualitative excitation profile as previous calculations) will not be discussed in detail: Focus will be put on the β -dipeptide and tripeptide, but all excitation energies and assignments are included in the supporting information⁵³. The model peptides display local excitations of $n \rightarrow \pi$ character within the carbonyl groups and of $\pi \rightarrow \pi^*$ character between the carbonyl and peptide bonds (denoted “W” and “NV” in ref. 46). Seeing that the $\pi \rightarrow \pi^*$ “NV” type of excitations have been left out from the study of Peach *et al.*⁴³ we will only briefly discuss them here. These excitations have also been removed from Table I (see ref. 53) and they will not be included in the statistical analysis in Section IV C. The peptide models further display two different kinds of charge transfer excitations: either these involve the peptide $\pi \rightarrow \pi^*$ systems (“CT₁”) or the carbonyl $n \rightarrow \pi^*$ lone pairs (“CT₂”). In the dipeptide the local carbonyl $n_1 \rightarrow \pi^*$ and $n_2 \rightarrow \pi^*$ excitations occur in the same order for TD-MC-srPBE and CASPT2. However, this changes for the β -dipeptide where the two local transitions occur in reversed order at the TD-MC-srPBE level, compared to the CASPT2 results.⁵³ The reversed ordering of these two excitations in the β -dipeptide corresponds to what is obtained by B3LYP and CAM-B3LYP functionals. We note that the inversion of excitations in the β -peptide also occurs for $\pi \rightarrow \pi^*$ type of excitations

TABLE I. Vertical excitation energies (in eV). "sr" is shorthand for "srPBE"

Molecule	Assign.	Type	TD-HF	TD-HF-sr	SOPPA	SOPPA-sr	TD-MC-sr	TD-B3LYP	TD-CAM-B3LYP	Ref
Dipeptide	$n_1 \rightarrow \pi_1^*$	L	6.55	6.41	5.01	5.53	5.61	5.55	5.68	5.62 ^a
Dipeptide	$n_2 \rightarrow \pi_2^*$	L	6.78	6.64	5.22	5.75	5.83	5.77	5.92	5.79 ^a
Dipeptide	$\pi_1 \rightarrow \pi_2^*$	CT ₁	8.44	7.47	6.58	6.95	7.59	6.15	7.00	7.18 ^a
Dipeptide	$n_1 \rightarrow \pi_{N2}^*$	CT ₂	8.98	7.60	6.85	7.10	8.10	6.31	7.84	8.07 ^a
PP	$\pi_1 \rightarrow \pi_1^*$	L	5.83	5.20	4.26	4.97	5.40	4.76	5.06	4.85 ^b
PP	$\pi_2 \rightarrow \pi_2^*$	L	5.41	5.31	4.55	5.04	5.48	4.96	5.12	5.13 ^b
PP	$\pi_1 \rightarrow \pi_2^*$	CT	5.57	5.68	4.99	5.25	5.70	4.58	5.27	5.47 ^b
PP	$\pi_2 \rightarrow \pi_1^*$	CT	7.40	6.89	5.57	5.84	6.65	4.64	5.92	5.94 ^b
DMABN	$\pi_1 \rightarrow \pi_{CN}^*$	L	5.41	4.88	3.87	4.56	5.09	4.44	4.72	4.25 ^c
DMABN	$\pi_2 \rightarrow \pi_{CN}^*$	CT	5.22	5.06	4.14	4.73	5.12	4.64	4.91	4.56 ^c

^aCASPT2 results from Serrano-André and Fülcher⁴⁶^bCC2 results from Peach *et al.*⁴³^cGas phase experiment from Bulliard *et al.*⁴⁷

TABLE II. Vertical excitation energies (in eV). "sr" is shorthand for "srPBE"

Molecule	Assign.	Assignment	TD-MC-sr	TD-B3LYP	TD-CAM-B3LYP	Ref
β -Dipeptide	$n_2 \rightarrow \pi_2^*$	L	5.60	5.56	5.67	5.40 ^a
β -Dipeptide	$n_1 \rightarrow \pi_1^*$	L	5.74	5.66	5.76	5.10 ^a
β -Dipeptide	$\pi_1 \rightarrow \pi_{N2}^*$	CT ₁	7.41	7.2	8.01	7.99 ^a
β -Dipeptide	$n_1 \rightarrow \pi_2^*$	CT ₂	8.21	7.26	8.38	9.13 ^a
Tripeptide	$n_1 \rightarrow \pi_1^*$	L	5.66	5.57	5.72	5.74 ^a
Tripeptide	$n_3 \rightarrow \pi_3^*$	L	5.87	5.74	5.93	5.61 ^a
Tripeptide	$n_2 \rightarrow \pi_2^*$	L	5.92	5.88	6.00	5.92 ^a
Tripeptide	$\pi_1 \rightarrow \pi_2^*$	CT ₁	8.12	6.27	6.98	7.01 ^a
Tripeptide	$\pi_2 \rightarrow \pi_3^*$	CT ₁	8.31	6.60	7.69	7.39 ^a
Tripeptide	$\pi_1 \rightarrow \pi_{N3}^*$	CT ₁	8.43	6.06	8.51	8.74 ^a
Tripeptide	$n_1 \rightarrow \pi_{N2}^*$	CT ₂	8.52	6.33	7.78	8.12
Tripeptide	$n_2 \rightarrow \pi_{N3}^*$	CT ₂	8.84	6.83	8.25	8.33
Tripeptide	$n_1 \rightarrow \pi_3^*$	CT ₂	9.04	6.12	8.67	9.30
HCl	¹ Π	CT	8.03	7.65	7.79	8.23 ^b

^aCASPT2 results from Serrano-André and Fülcher, ref. 46^bCC2 results from Peach *et al.*⁴³

("NV₁(1)" and "NV₁(2)" in ref. 46). We thus obtain NV₁(2) as the lowest of the two excitations.

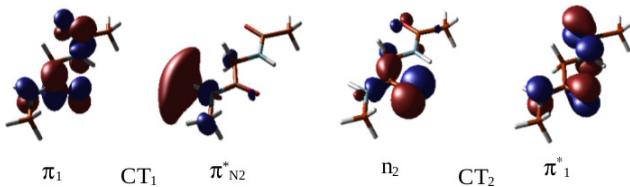


FIG. 3. Orbitals involved in the two charge transfer excitations in the dipeptide.

In the tripeptide, the lowest TD-MC-srPBE excita-

tions are the local intra carbonyl excitations, which is in agreement with the reference CASPT2 results, but the order of the two first excitations are again reversed. This inversion is also observed at both TD-B3LYP and TD-CAM-B3LYP levels. The three NV₁ excitations seem to come in the same order as in CASPT2, although this cannot be unequivocally verified since the first two are nearly degenerate. A word of caution is also necessary for the classification of the charge transfer excitations. We find that the accepting orbitals occasionally are mainly located at the peptide N–H bond as shown in Figure 3 (using the dipeptide as example). These kinds of accepting orbitals are denoted " π_N " orbitals in Table I and Table II.

It should finally be mentioned that we seem to experience more mixing of states in our TD-MC-srPBE calculations than in the reference CASPT2 calculations⁴⁶. One reason for this might be that the CASPT2 benchmarks were performed with an ANO type basis of double zeta quality, whereas we have used the more extensive cc-pVTZ. The use of different sized basis sets might also be the reason for the inversion of states described above.

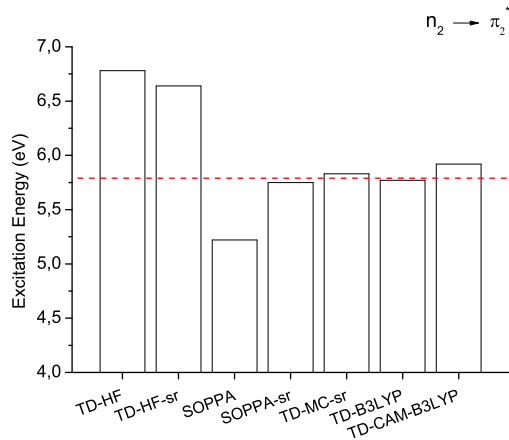


FIG. 4. Local excitation in the model dipeptide. The red dotted line is the CASPT2 results from ref. 46. “sr” is short-hand for “srPBE”.

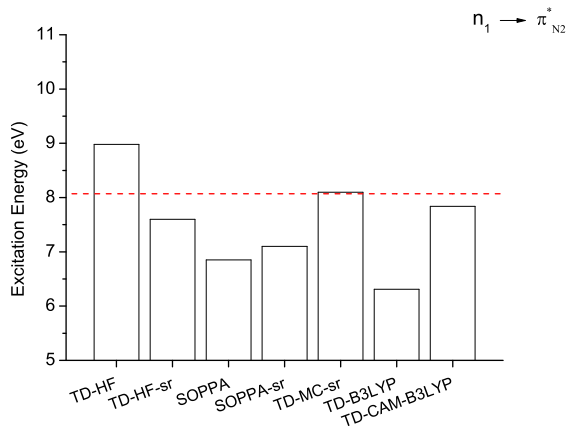


FIG. 5. Charge transfer excitation in the model dipeptide. The red dotted line is the CASPT2 results from ref. 46. “sr” is short-hand for “srPBE”.

B. Comparing SOPPA-srPBE with TD-MC-srPBE results

The subset of molecules considered in this section is given in Table I, where also the results are compiled. For the dipeptide, the performance of the various methods is depicted in Figures 4 and 5 for the $n_2 \rightarrow \pi_2^*$ (“W₂”) and the charge transfer (“CT₂”) transitions, respectively. As

expected the local transitions are overestimated at the TD-HF level and we expect a similar situation within regular TD-MCSCF (a good estimate for this overestimation is provided by considering *e.g.* the results from state-averaged CASSCF from ref. 48 which is about 1.4 eV too high for the DMABN molecule). TD-HF-srPBE leads to a change in the right direction, but it is not sufficient to obtain agreement with the reference CASPT2 values. SOPPA significantly underestimates the local carbonyl excitations while SOPPA-srPBE is very close to the CASPT2 values for the local $n_1 \rightarrow \pi_1^*$ (“W₁”) and $n_2 \rightarrow \pi_2^*$ (“W₂”) excitations. The TD-MC-srPBE model also remedies the tendency to overestimate excitation energies from the MCSCF type of wave functions and the two local excitations are obtained very accurately. Both TD-B3LYP and TD-CAM-B3LYP are, as expected, also of high accuracy for these two excitations. Moving to the charge transfer excitations, both Table I and Figure 5 show that these are severely underestimated by the B3LYP functional in the dipeptide. The CAM-B3LYP functional provides slightly better results, which is not surprising as its parameters have been optimized for reproducing such excitations well. TD-HF and SOPPA behave similarly as for the local excitations and thus overestimate and underestimate, respectively, the charge transfer excitations. Note that, for the charge transfer “CT₂”, TD-HF-srPBE is closer to CASPT2 than SOPPA-srPBE, even though the latter performs better than SOPPA. The TD-MC-srPBE method is also for charge transfer excitations very accurate and for the dipeptide it even outperforms CAM-B3LYP.

We can from the discussion for the dipeptide also comment on some general trends in Table I. As documented many times before, TD-HF overestimates both charge transfer and local excitations and the TD-HF-srPBE method generally brings the result closer to the reference data. However, the correspondence is still not satisfactory for the method to be of use for quantitative treatments, as it neglects long-range correlation effects. The regular SOPPA model generally underestimates both local and charge transfer excitations, while the SOPPA-srPBE method is a significant improvement for both types of excitations in all molecules considered. The TD-MC-srPBE method is often an improvement compared to TD-HF and also to TD-HF-srPBE. For charge transfers, TD-MC-srPBE is in general also an improvement to B3LYP and occasionally even to CAM-B3LYP. One notable exception is the DMABN molecule, where B3LYP previously has been noted to perform well, also for charge-transfer excitations⁵⁴. In the following section the TD-MC-srPBE method is further tested against the above-mentioned functionals, using the full test set in Figure 1.

Considering the present selection of molecules, our initial study reveals promising results for the SOPPA-srPBE method. The method is a viable alternative to TD-MC-srPBE, showing often similar or even better accuracy, in particular for the DMABN and PP molecules.

However, it should be noted that the molecules within the current test set are at large dominated by a single configuration and the present accuracy is not expected to extend to molecules exhibiting multiconfigurational character in their electronic ground state.

C. Performance of TD-MC-srPBE on the full molecular test set

The inclusion of the inorganic diatom HCl, the β -dipeptide and the tripeptide for testing the performance of the TD-MC-srPBE method yields a total of 24 singlet excitations; 14 of these have charge transfer character and 10 are local. This test set is still not very extensive but we believe it is sufficiently large to compare TD-MC-srPBE with B3LYP and CAM-B3LYP performances on a reasonable statistical basis. For the full benchmark

TABLE III. Error analysis for 24 excitations described in text. “sr” is short-hand for “srPBE”. All errors are given in eV

	TD-MC-sr	TD-B3LYP	TD-CAM-B3LYP
Mean	0.23	-0.76	-0.01
std. dev.	0.48	0.97	0.33
MAD	0.42	0.86	0.25
std. dev.	0.31	0.86	0.21

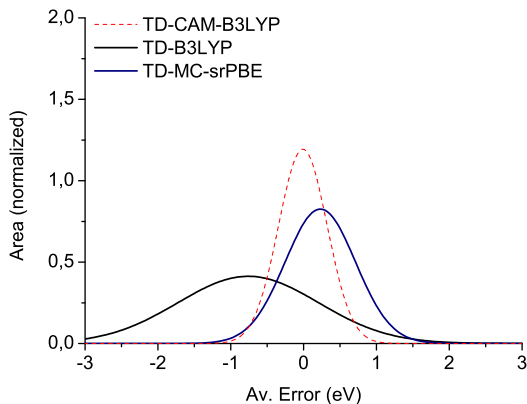


FIG. 6. Normal distribution from data in Table III. centered around the mean deviation.

set, including both local and charge transfer excitations, the statistical parameters are given in Table III and the normal distributions are shown in Figure 6. The TD-MC-srPBE method generally shows good performance over the whole set, even with the moderate active spaces used here. In this aspect it is worthwhile to notice that the CASPT2 reference calculations for the peptide model systems used a significantly larger active space (although

TABLE IV. Error analysis for 14 CT excitations described in text. “sr” is short-hand for “srPBE”. All errors are given in eV

	TD-MC-sr	TD-B3LYP	TD-CAM-B3LYP
Mean	0.19	-1.34	-0.18
std. dev.	0.58	0.86	0.29
MAD	0.51	1.36	0.27
std. dev.	0.31	0.85	0.22

also a smaller basis set). The CAM-B3LYP functional is the most accurate with a very small mean deviation of -0.01 eV. Also the mean absolute deviation (MAD) is the smallest for CAM-B3LYP. B3LYP is significantly off as expected due to the charge transfer type of excitations. If focus is solely on these type of excitations, the error of B3LYP is even more pronounced, as shown from the statistical analysis result over the charge transfer excitations in Table IV (the normal distributions are displayed in Figure 7). B3LYP now (on average) underestimates the

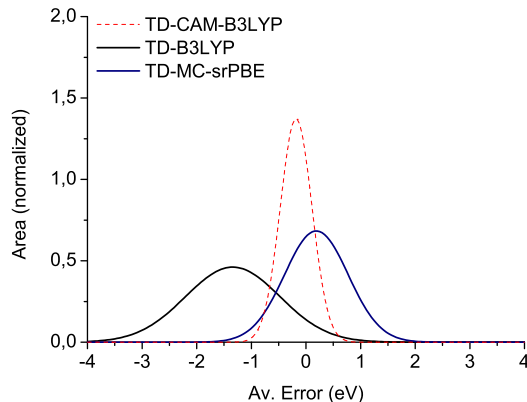


FIG. 7. Normal distribution from data in Tables IV (CT excitations) centered around the mean deviation.

vertical excitations by -1.34 eV, whereas CAM-B3LYP still underestimates CT type excitations, but with a considerable smaller margin. TD-MC-srPBE is here comparable to CAM-B3LYP (although the MAD is somewhat higher) and it seems that in general the srPBE functional remedies the commonly encountered overestimation of excitation energies at the MCSCF level. For completion the results from the local excitations are given in Table V and Figure 8. B3LYP is here on average the closest to the reference data (the deviation is 0.05 eV). It is noteworthy that TD-MC-srPBE is still accurate, although not as accurate as B3LYP and CAM-B3LYP. As it was the case for SOPPA-srPBE it should be noted that the use of B3LYP and CAM-B3LYP will be problematic for molecules showing significant multireference and/or double excitation character.

TABLE V. Error analysis for 10 local excitations described in text. “sr” is short-hand for “srPBE”. All errors are given in eV

	TD-MC-sr	TD-B3LYP	TD-CAM-B3LYP
Mean	0.28	0.05	0.22
std. dev.	0.31	0.22	0.22
MAD	0.30	0.16	0.22
std. dev.	0.29	0.15	0.21

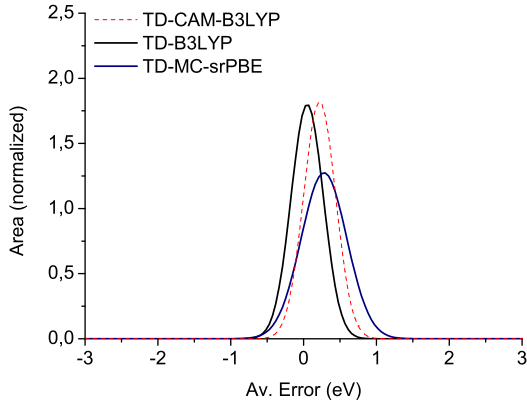


FIG. 8. Normal distribution from data in Table V (Local excitations) centered around the mean deviation.

D. The retinal chromophore

As a final test case, we applied the TD-MC-srPBE method to the calculation of the low-lying singlet excited state spectrum of the retinal chromophore. This chromophore displays significant multireference character in its ground state, whereas the low-lying singlet excitations are dominated by a double excitation character, which cannot be described by regular TD-DFT (within the common adiabatic approximation). The natural orbitals spanning the chosen CAS(6,6) space are shown in Figure 9 and display the expected increase in nodal planes as one moves from orbitals of high occupation numbers (π_1 – π_3) towards orbitals of lower occupation numbers (π_4^* – π_6^*). Before discussing the excitation energies in detail, a technical aspect concerning the choice of active space in TD-MC-srPBE is addressed. A well-known problem with including dynamical correlation on top of a multireference method (for example CASSCF/CASPT2) is that it can lead to intruder states or root flipping. In MC-srDFT dynamical and static correlations are treated simultaneously, which often means that an active space can be used that is significantly smaller than the one of a regular MCSCF calculation. This beneficial feature is illustrated by the MP2-srPBE and MP2 (in parentheses) natural orbital occupation numbers of the three highest

occupied orbitals shown in Figure 9. Similar differences between MP2 and MP2-srPBE have been observed for all molecules considered in this study, and a comparison of MP2 and MP2-srPBE occupation numbers is given in the supporting information for the full test set⁵³

Our excitation energies for the retinal chromophore computed at the TD-MC-srPBE level are compiled in Table VI. As can be seen from Table VI the singlet excited states S_1 and S_2 are well separated and the first state is the bright state with a large oscillator strength whereas the second state is the dark state with a considerably lower oscillator strength. Using the nomenclature from polyenes, the S_1 state thus corresponds to the B_u state while the second state S_2 is the A_g state, which is in agreement with both experiment^{55–57} and previous CASPT2 results⁵⁸ using the same basis set. Quantitatively, the $S_0 \rightarrow S_1$ excitation is in good agreement with previous CASPT2 and other theoretical results (c.f. footnote *a* in Table VI). We note that the experimental value given here is the gas-phase value, while we have used a geometry obtained in an optimization considering also the surrounding protein (the calculation itself does *not* include the protein environment) taken from a forthcoming publication. Thus one should not expect a one-to-one correspondence which should be kept in mind when considering the $S_0 \rightarrow S_2$ excitation energy. The latter is slightly overestimated by 0.41 eV at the TD-MC-srPBE level compared to the experimental gas-phase value but also to the theoretical value of Altun and co-workers⁵⁹). However, the agreement with theory must be still considered reasonable in light of employing slightly different retinal models, quantum mechanical methods as well as geometry optimization conditions.

TABLE VI. Excitation energies for the retinal chromophore (eV) with oscillator strengths in parentheses. “sr” is short-hand for “srPBE”.

Excitation	TD-MC-sr	DDCI2 + Q ^a	Exp.
$S_0 \rightarrow S_1$	2.29 (1.597)	2.27 ⁵⁹	2.03 ⁵⁶
$S_0 \rightarrow S_2$	3.63 (0.522)	3.07 ⁵⁹	3.22 ⁵⁷

^aThe DDCI2 calculations were performed with an underlying CAS(12,12). For the for $S_0 \rightarrow S_1$ excitation CASPT2(12,12) obtains 2.32 eV⁵⁸ while B3LYP obtains 2.48⁶⁰ eV.

The retinal calculations nicely illustrate an important aspect of the TD-MC-srPBE method. Both the $S_0 \rightarrow S_1$ and the $S_0 \rightarrow S_2$ excitations have a considerable doubly-excited character, as indicated by the significant weight of configuration **3** (red) in the charts of Figure 9 (for the linear response coefficient of this configuration, see the accompanying table on the left-hand side of Figure 9). Indeed, this weight is so important in the $S_0 \rightarrow S_2$ transition that the latter can be considered as a two-electron $\pi_3 \rightarrow \pi_4^*$ excitation. TD-DFT based on its standard adiabatic approximation formulation cannot describe such a transition, ultimately missing the electronic nature of

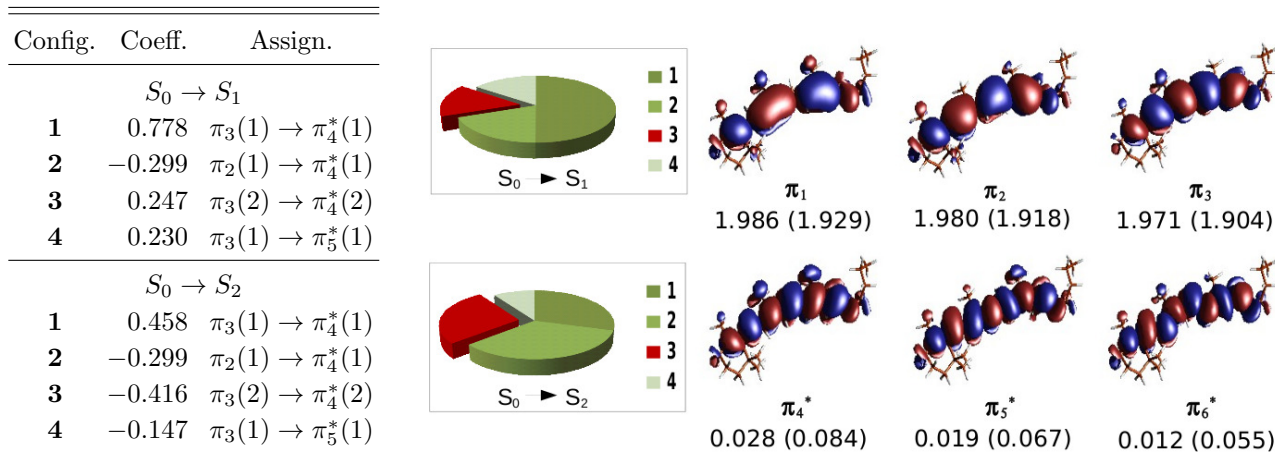


FIG. 9. Orbitals within the active space for the retinal chromophore in Figure 2. Numbers under the orbitals are the MP2-srPBE natural orbital occupancies. Regular MP2 occupancies are in parentheses. The table at the left-hand side shows linear response coefficients for the dominant configurations, 1–4. The numbers in parentheses are the number of involved electrons. The chart shows the relative contributions of 1–4 for both the $S_0 \rightarrow S_1$ and $S_0 \rightarrow S_2$ excitations, where the red (3) is double excitation character.

the dark state. It should be noted that the present study lacks the effect from the protein environment which can be significant as studies by Söderhjelm *et al.* have shown⁶¹. Work to incorporate the effect from the environment into our TD-MC-srDFT model is currently in progress based on the polarizable-embedding method by Kongsted and co-workers^{62,63}.

V. CONCLUSION

In this paper the SOPPA-srDFT method has been formulated and tested together with the recently presented TD-MC-srDFT approach using a srPBE functional for the srDFT part. We have compared the performance of these methods to standard TD-DFT using B3LYP and CAM-B3LYP functionals for excitation energies, using a model peptide, *N*-phenyl pyrrole (PP) and 4-(*N,N*-dimethylamino) benzonitrile (DMABN) as test cases. The assessment has been done with explicit focus on charge-transfer excitations although results for local excitations have been included as well. While the regular SOPPA method underestimates both local and charge-transfer excitations, SOPPA-srPBE is generally much closer to the reference CASPT2 data. Considering the total benchmark set of 24 excitations (from molecules in Figure 1) TD-DFT/CAM-B3LYP still performs best whereas due to the large discrepancies in the charge-transfer excitations, TD-DFT/B3LYP cannot be recommended for a general application to excitation energies of various characters. The TD-MC-srPBE method commonly yields sufficiently accurate charge-transfer excitation energies while in some cases it even outperforms TD-DFT/CAM-B3LYP. Notably, this accuracy can not only be achieved with quite small active spaces for the long-range-interacting CASSCF wave function but the

MC-srDFT *ansatz* also scales nearly with respect to system size compared to regular MCSCF.

Doubly-excited (singlet) states cannot be described with regular TD-DFT schemes if they rely on the popular adiabatic approximation. The TD-MC-srPBE method on the other hand does not suffer from this shortcoming by design since double excitation can be effectively described within the long-range MCSCF part of the wave function. In order to illustrate this important capability, we have here investigated the retinal chromophore as a prime example of (bio-)chemical interest where double excitations play a major role in the photophysics of the low-lying excited states. Our present results for the excitation energies of the first two singlet excited states are promising and within the range of previously reported CASPT2 and MRCI data, albeit the fact that the latter methods required much larger active spaces. To further enhance the scope of TD-MC-srDFT applications we currently address the computation of properties which are not easily implemented for CASPT2 type wave functions (such as NMR parameters). An extension of the TD-MC-srDFT approach to embedding into solvent or protein environments is in progress in our laboratories.

ACKNOWLEDGMENTS

E.D.H. thanks OTICON and Augustines funds for stipends. The authors wish to thank the Danish Center for Scientific Computing for computational resources. S.K. acknowledges the Danish Natural Science Research Council for an individual postdoctoral grant (10-082944). E.F. thanks ANR (DYQUMA project).

¹M. Grätzel, Acc. Chem. Res., **14**, 376 (1981).

²D. Gust, T. A. Moore, and A. L. Moore, Acc. Chem. Res., **42**, 1890 (2009).

- ³E. Runge and E. K. U. Gross, *Phys. Rev. Lett.*, **52**, 997 (1984).
- ⁴M. A. L. Marques and E. K. U. Gross, *Annu. Rev. Phys. Chem.*, **55**, 427 (2004).
- ⁵M. Casida and M. Huix-Rotllant, *Annu. Rev. Phys. Chem.*, **63**, 287 (2012).
- ⁶D. J. Tozer, R. D. Amos, N. C. Handy, B. Roos, and L. Serrano-Andrés, *Mol. Phys.*, **97**, 859 (1999).
- ⁷M.-S. Liao, Y. Lu, and S. Scheiner, *J. Comput. Chem.*, **24**, 623 (2003).
- ⁸E. Fabiano, F. Della Sala, G. Barbarella, S. Lattante, M. Anni, G. Sotgiu, C. Hättig, R. Cingolani, and G. Gigli, *J. Phys. Chem. B*, **110**, 18651 (2006).
- ⁹E. Perpète, J. Preat, J.-M. André, and D. Jacquemin, *J. Phys. Chem. A*, **110**, 5629 (2006).
- ¹⁰A. Dreuw and M. Head-Gordon, *J. Am. Chem. Soc.*, **126**, 4007 (2004).
- ¹¹O. A. Vydrov and G. E. Scuseria, *J. Chem. Phys.*, **125**, 234109 (2006).
- ¹²M. A. Rohrdanz, K. M. Martins, and J. M. Herbert, *J. Chem. Phys.*, **130**, 054112 (2009).
- ¹³R. Baer, E. Livshits, and U. Salzner, *Annu. Rev. Phys. Chem.*, **61**, 85 (2010).
- ¹⁴T. Yanai, D. P. Tew, and N. C. Handy, *Chem. Phys. Lett.*, **393**, 51 (2004).
- ¹⁵N. T. Maitra, F. Zhang, R. J. Cave, and K. Burke, *J. Chem. Phys.*, **120**, 5932 (2004).
- ¹⁶J. Neugebauer, E. J. Baerends, and M. Nooijen, *J. Chem. Phys.*, **121**, 6155 (2004).
- ¹⁷P. Elliot, S. Goldson, C. Canahui, and N. T. Maitra, *Chem. Phys.*, **391**, 110 (2011).
- ¹⁸K. Burke, *J. Chem. Phys.*, **136**, 150901 (2012).
- ¹⁹K. Andersson, P.-Å. Malmqvist, B. O. Roos, A. J. Sadlej, and K. Wolinski, *J. Phys. Chem.*, **94**, 5483 (1990).
- ²⁰K. Andersson, P.-Å. Malmqvist, and B. O. Roos, *J. Chem. Phys.*, **96**, 1218 (1992).
- ²¹C. Angeli, R. Cimiraglia, S. Evangelisti, T. Leininger, and J.-P. Malrieu, *J. Chem. Phys.*, **114**, 10252 (2001).
- ²²S. Grimme and M. Waletzke, *J. Chem. Phys.*, **111**, 5645 (1999).
- ²³C. M. Marian and N. Gilka, *J. Chem. Theory Comput.*, **4**, 1501 (2008).
- ²⁴J. G. Ángyán, I. C. Gerber, A. Savin, and J. Toulouse, *Phys. Rev. A*, **72**, 012510 (2005).
- ²⁵E. Fromager and H. J. Aa. Jensen, *Phys. Rev. A*, **78**, 022504 (2008).
- ²⁶T. Leininger, H. Stoll, H.-J. Werner, and A. Savin, *Chem. Phys. Lett.*, **275**, 151 (1997).
- ²⁷E. Goll, H.-J. Werner, and H. Stoll, *Phys. Chem. Chem. Phys.*, **7**, 3917 (2005).
- ²⁸E. Fromager, J. Toulouse, and H. J. Aa. Jensen, *J. Chem. Phys.*, **126**, 074111 (2007).
- ²⁹E. Fromager, F. Réal, P. Wählin, U. Wahlgren, and H. J. Aa. Jensen, *J. Chem. Phys.*, **131**, 054107 (2009).
- ³⁰E. Fromager, R. Cimiraglia, and H. J. Aa. Jensen, *Phys. Rev. A*, **81**, 024502 (2010).
- ³¹K. Pernal, *J. Chem. Phys.*, **136**, 184105 (2012).
- ³²E. Fromager, S. Knecht, and H. J. Aa. Jensen, *J. Chem. Phys.*, **138**, 084101 (2013).
- ³³E. Rebolini, A. Savin, and J. Toulouse, *Mol. Phys.* (2013), doi: 10.1080/00268976.2013.794313.
- ³⁴N. Ferré and M. Olivucci, *J. Am. Chem. Soc.*, **12**, 6868 (2003).
- ³⁵A. Savin, "Recent developments and applications of modern density functional theory," (Elsevier, Amsterdam, 1996) p. 327.
- ³⁶J. Toulouse, F. Colonna, and A. Savin, *Phys. Rev. A*, **70**, 062505 (2004).
- ³⁷O. Christiansen, P. Jørgensen, and C. Hättig, *Int. J. Quantum Chem.*, **68**, 1 (1998).
- ³⁸J. Olsen and P. Jørgensen, *J. Chem. Phys.*, **82**, 3235 (1985).
- ³⁹T. Saue and H. J. Aa. Jensen, *J. Chem. Phys.*, **118**, 522 (2003).
- ⁴⁰J. Oddershede, P. Jørgensen, and D. L. Yeager, *Comput. Phys. Rep.*, **2**, 33 (1984).
- ⁴¹M. J. Peach, E. K. Dalskov, T. Enevoldsen, H. J. Aa. Jensen, and J. Oddershede, *J. Chem. Phys.*, **105**, 5886 (1996).
- ⁴²E. Fromager and H. J. Aa. Jensen, *J. Chem. Phys.*, **135**, 034116 (2011).
- ⁴³M. J. Peach, P. Benfield, T. Helgaker, and D. J. Tozer, *J. Chem. Phys.*, **128**, 044118 (2008).
- ⁴⁴X. Xu, Z. Cao, and Q. Zhang, *J. Phys. Chem. A*, **110**, 1740 (2006).
- ⁴⁵B. Proppe, M. Merchán, and L. Serrano-Andrés, *J. Phys. Chem. A*, **104**, 1608 (2000).
- ⁴⁶L. Serrano-Andrés and M. P. Fülscher, *J. Am. Chem. Soc.*, **120**, 10912 (1998).
- ⁴⁷C. Bulliard, M. Allan, G. Wirtz, E. Haselbach, K. Zachariasse, N. Detzer, and S. Grimme, *J. Phys. Chem. A*, **103**, 7766 (1999).
- ⁴⁸D. Rappoport and F. Furche, *J. Am. Chem. Soc.*, **124**, 2277 (2004).
- ⁴⁹L. Serrano-Andrés, M. Merchán, B. O. Roos, and R. Lindh, *J. Am. Chem. Soc.*, **117**, 3189 (2013).
- ⁵⁰T. H. Dunning Jr., *J. Chem. Phys.*, **90**, 1007 (1989).
- ⁵¹K. Sneskov, T. Olsen, M. J. Schwabe, C. Hättig, O. Christiansen, and J. Kongsted, *Phys. Chem. Chem. Phys.*, **in press** (2013).
- ⁵²"Dalton, a molecular electronic structure program, release dalton2011 (2011), see <http://daltonprogram.org/>," development version (2011).
- ⁵³See supplementary material for a full table of TD-MC-srPBE excitation energies, including all used reference values. The supplementary material also contains MP2 and MP2-srPBE occupation numbers for the used test set.
- ⁵⁴C. Jamorski, J. B. Foresman, C. Thilgen, and H.-P. Lüthi, *J. Chem. Phys.*, **116**, 8761 (2002).
- ⁵⁵R. R. Birge and C.-F. Zhang, *J. Chem. Phys.*, **92**, 7178 (1990).
- ⁵⁶L. H. Andersen, I. B. Nielsen, M. B. Kristensen, M. O. A. El Ghazaly, S. Haacke, M. B. Nielsen, and M. Å. Petersen, *J. Am. Chem. Soc.*, **127**, 12347 (2005).
- ⁵⁷I. B. Nielsen, L. Lammich, and L. H. Andersen, *Phys. Rev. Lett.*, **96**, 018304 (2006).
- ⁵⁸A. Cembran, R. González-Luque, P. Altoé, M. Merchán, F. Bernardi, M. Olivucci, and M. Garavelli, *J. Phys. Chem. A*, **109**, 6597 (2005).
- ⁵⁹A. Altun, S. Yokoyama, and K. Morokuma, *J. Phys. Chem. B*, **112**, 16883 (2008).
- ⁶⁰T. Vreven and K. Morokuma, *Theor. Chem. Acc.*, **109**, 125 (2003).
- ⁶¹P. Söderhjelm, C. Husberg, A. Strambi, M. Olivucci, and U. Ryde, *J. Chem. Theory Comput.*, **5**, 649 (2009).
- ⁶²J. M. Olsen, K. Aidas, and J. Kongsted, *J. Chem. Theory and Comput.*, **6**, 3721 (2010).
- ⁶³J. M. Olsen and J. Kongsted, *Adv. Quant. Chem.*, **61**, 107 (2011).